Inserts in a Multiple-Column Format

GARY BENSON, DEBI ERPENBECK, AND JANET HOLMES

Gary Benson
MS D417
Los Alamos, NM 87545
gsb@lanl.gov

Debi Erpenbeck
MS D418
Los Alamos, NM 87545
dje@lanl.gov

Janet Holmes
MS D417
Los Alamos, NM 87545
jah@lanl.gov

ABSTRACT

A few years ago, we approached the problem of placing inserts (or "objects") automatically in a multiple-column format. Among the issues we encountered were enabling users to place an object wherever they desired following a textual reference (the "place-it-here" option); placing objects that spanned columns into a page while maintaining text flow in a one-pass system; and creating a text-flow pattern that followed the style of the physics journal *Physical Review*. We use a stack-like method of storing objects to create solutions to these problems.

1. Introduction

In October 1986 we became intrigued by the problems caused when inserts or objects, such as figures and equations, must be placed within a multiple-column TEX format. Such text/figures/equations formats are common in documents we process at Los Alamos National Laboratory in our composition section. Therefore, we felt we had to find a (hopefully simple) way to solve the figure-placement (or insert-placement) problem within TEX. The goal of our first attempts was to place inserts at the top and bottom of pages in a three-column report format.

We were able to complete the TEX coding required to solve this first problem in about forty hours and produced the desired results. However, reports designed by various groups at Los Alamos required different insert-placement rules — frequently ones that would not permit the simple top or bottom insertion. At this point, therefore, our thoughts turned to the larger problem of placing inserts either after a textual reference or down and to the right of a reference. Because of other work assignments, we produced only design notes and sketches at first. In February 1989, however, we received a request from the editors working on a journal at Los Alamos for TEX macros that would direct the placement of inserts according to the style of the *Physical Review* in a two-column format. This gave us the opportunity to work with insert-placement rules considerably more complex than our original problem.

2. Definition of the Problem

The *Physical Review* format requires that several basic rules be followed. These are:

1. Material must be easily included into multiple-column (in this case two-column) text.
2. The insert must always follow the textual reference to it, which means that, depending on its position within the article, it could conceivably fall at the top of a page, at the bottom, or anywhere

0 — the page number that is currently being processed
user specified — in which case the program will try to place the insert on the specified page
Note: this does not apply to "place-it-here"-type objects; see item 6 below.

4. `\endmulcolinsert` . Shows where the inserted object ends and places the object on the stack.
5. `\balancetothispoint` . This macro balances the material that TEX is going to put on the current page between two columns and makes a top insert of the balanced material.
6. `\refinsertadj`=*a dimension value* . Use this macro to position a "place-it-here" object after its reference. We found that, in some cases, an object is not placed correctly (for example, between the word "Figure" and the number "1" with each on a separate line). This macro is a "fudge factor" to ensure proper placement in such cases, and goes before the `\beginmulcolinsert` macros.

The above macros required a few additions to format articles according to the *Physical Review* specifications. Notably, *Physical Review* uses reading flow indicators, or "reader bars," to guide the reader's eye in the direction of text when the text flow is interrupted by a figure or equation that spans two columns. We show an example of *Physical Review* page layout using these reader bars in Sec. 4, examples 3 and 4. The additional macros supporting a *Physical Review*-style format are given below.

1. `\phyrevtrue` . This draws reading flow indicators when a `\balancetothispoint` macro is encountered. It draws ⌋ to indicate that the text above the line is a section and draws ⌈ to indicate that the text below the line is a section.
2. `\phyrevfalse` . This cancels the effect of `\phyrevtrue` .
3. `\noclubtextlines`{n}, where n is the number of lines of text ("club lines") allowed to sit by themselves in a column below an insert. At Los Alamos, we usually require five or more lines to appear in such a position, so the `\noclubtextlines` argument would be 5.
4. `\copy\upreadbarbox` . This sequence of commands creates an upward-pointing reader bar at the position specified in the text.
5. `\copy\downreadbarbox` . Likewise, this sequence of commands creates a downward-pointing reader bar at the position specified in the text.

3.4 Design and Implementation Concerns

The coding for the macros listed in Section 3.3 required about 100 hours. Up to ten objects can be stored on the stack at one time. Only versions of TEX that have their registers doubled can process code using these macros; i.e., Sun and VAX systems.

Early in the design we realized that users may mistake features of these macros for bugs and that, to avoid user confusion, we'd better document what the code does *not* do as well as what it does do. For example, take the case of an object that is referenced in the right column but spans two columns. This situation will process correctly only if there are no multiple-column-spanning objects already in place that had been referenced in the left column. (This is a one-pass system, remember.) With this macro package, the program will place the object referenced in the right column on the next page.

We divided the processing code so that it would be easy to introduce new coding and allow fault (bug) detection. Some of the bugs we suspected were not bugs, but resulted from our inability to foresee results. There were, as usual, a number of typos and "why did I do that?"-type problems. However, there are still several elusive bugs that need to be found. For example, the following conditions occurring together in a document cause some text to be dropped:

1. The first page of the document contains a `\balancetothispoint`, which creates an object containing text and graphics that is placed on the stack as a top object. The next object is an equation.
2. The second page of the document contains two top and two bottom objects. `\noclubtextlines` is set to 5 to avoid club text at midpage.
3. The third page, like the first, contains a `\balancetothispoint`, creating an object containing text and graphics that is placed on the stack as a top object, and an equation follows as the next object. However, text is suddenly missing from the top of this page. We've worked around this situation by placing the two top and two bottom objects from the second page within a full-page object, but this fix seems clumsy.

4. Examples

4.1 Example 1: A Simple Example

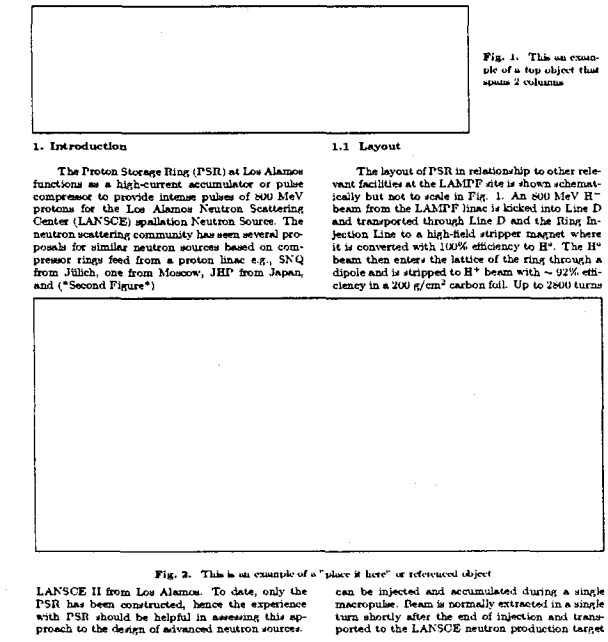

Fig. 1. This an example of a top object that spans 2 columns

1. Introduction

The Proton Storage Ring (PSR) at Los Alamos functions as a high-current accumulator or pulse compressor to provide intense pulses of 800 MeV protons for the Los Alamos Neutron Scattering Center (LANSCE) spallation Neutron Source. The neutron scattering community has seen several proposals for similar neutron sources based on compressor rings feed from a proton linac e.g., SNQ from Jülich, one from Moscow, JHP from Japan, and (*Second Figure*)

1.1 Layout

The layout of PSR in relationship to other relevant facilities at the LAMPF site is shown schematically but not to scale in Fig. 1. An 800 MeV H^- beam from the LAMPF linac is kicked into Line D and transported through Line D and the Ring Injection Line to a high-field stripper magnet where it is converted with 100% efficiency to H^0. The H^0 beam then enters the lattice of the ring through a dipole and is stripped to H^+ beam with ~ 92% efficiency in a 200 g/cm^2 carbon foil. Up to 2800 turns

Fig. 2. This is an example of a "place it here" or referenced object

LANSCE II from Los Alamos. To date, only the PSR has been constructed, hence the experience with PSR should be helpful in assessing this approach to the design of advanced neutron sources.

can be injected and accumulated during a single macropulse. Beam is normally extracted in a single turn shortly after the end of injection and transported to the LANSCE neutron production target

1

This is a simple example of a page with two inserted objects. The first is a top object and is placed automatically at the top of the page. The second is a "place it here" (or referenced) object that is placed about midway on the page after its reference in the text. (Note that the object is placed correctly after its reference.) The reference point is flagged by "(*Second Figure*)". The first part of the TEX code for this example is given below.

The first object's coding was placed before the start of the text. By coding this way, a compositor can group all the top and bottom objects in a report together in one place. Compositors like this feature because they tend to think of object placement in terms of "Fig. 1 at the top of page 5, Picture 3a at bottom of page 7," etc. However, because the number of objects that can be placed on a stack at any one time is ten, a report with more than ten inserts will require more than one grouping of top and bottom objects. Only the referenced objects must be embedded within text.

```
%
%       ex1.tex
%
\vsize=50pc                 % Set the vsize so macros know its value
\hsize=39pc                 % Set the hsize
\input mulcol2              % Load the mulcol/inserts macros
\input ex_macros            % Load the macros for the examples
\parskip=0pt

\beginmulcol{2}{18.5pc}     % Begin multiple columns
%
% First figure, a top object
%
\beginmulcolinsert{t}{2}{1}{1}
\lfigure{10pc}{30pc}{This an example of a top object that spans 2
columns}{}
\endmulcolinsert

\leftline{\bf I.~~INTRODUCTION}
The Proton Storage Ring (PSR) at Los Alamos functions as a high-current
accumulator or pulse compressor to provide intense pulses of 800 MeV
protons for the Los Alamos Neutron Scattering Center (LANSCE) spallation
Neutron Source.  The neutron scattering community has seen several
proposals for similar neutron sources based on compressor rings feed from a
proton linac e.g., SNQ from J\" ulich, one from Moscow, JHP from Japan, and
(*Second Figure*)
```

A portion of the log for example 2

```
 The insert starts in the left column
 and only spans the left column
>> Placing bottom insert number 4
 The insert starts in the right column
 and spans only the right column
>> Removing insert 3, from stack
>> Removing insert 4, from stack
>> [Finished page 2]
[3]
>> Processing insert number 9, to be placed on page 3
>> Processing insert number 10, to be placed on page 3
>> Processing insert number 11, to be placed on page 3
>> Processing insert number 12, to be placed on page 4
>> Processing insert number 13, to be placed on page 4
>> Processing insert number 14, to be placed on page 4
>> Insert 9, and reference moving to page 4
>> Insert 10, and reference moving to page 4
>> Insert 11, and reference moving to page 4
>> Insert 8, referenced in left column
 and spans the right column
>> Placing referenced insert number 8

Overfull \vbox (0.38889pt too high) has occurred while \output is active
>> Removing insert 8, from stack
>> [Finished page 3]
[4]
>> Insert 11, will not fit in left column
 Moving it to page 5, as a top insert and
 leaving the reference on the current page
>> Placing top insert number 7
 The insert starts in the right column
 and spans only the right column
>> Placing top insert number 6
 The insert starts in the left column
 and only spans the left column
>> Placing top insert number 5
 The insert starts in the left column
 and spans the right column
>> Placing bottom insert number 12
 The insert starts in the left column
 and only spans the left column
>> Placing bottom insert number 13
 The insert starts in the right column
 and spans only the right column
>> Placing bottom insert number 14
 The insert starts in the left column
>> Insert 9, referenced in left column
 and spans the right column
>> Placing referenced insert number 9
```

4.3 Example 3: What's Nice About the Fizzrev Shuffle.

This example illustrates the use of the macros to produce *Physical Review*-style documents and illustrates the advantage of using this style.

The example is broken up into two sections. The first section represents the output without using the *Physical Review* style; the second section shows the result of using this style. The example makes up a "before-and-after" sequence.

Before

5.1.8 Determination of Peak Position by a Linearized Gaussian Fit

This procedure transforms the Gaussian shaped peak into a line and then fits a line to the transformed peak. The slope and intercept of the fitted line are related to x_0 and σ. The background continuum under the peak is first subtracted so that

$$\sigma^2[y(x)] = y_i(x) - \frac{1}{4}\left[k^2\frac{H_h}{N_h^2} - (2-k)^2\frac{H_l}{N_l^2}\right] \qquad (5-17)$$

where

$$k = \frac{y(x - x_c)}{(x_h - x_c)} .$$

the fit is made only to the Gaussian-shaped peak.

Transformations that linearize the Gaussian function have been applied only recently to determine the parameters of gamma-ray peaks (Ref. 7). The simplest of a class of similar transformations is the function

$$Q(x) = ln\,\frac{y(x-1)}{y(x-1)} = \frac{2}{\sigma^2}\,x - \frac{2x_0}{\sigma^2} \qquad (5-11)$$

where $y(x)$ is the number of counts in channel x. The last expression in Equation 5-11 is correct if $y(x)$ is the usual Gaussian function. The linear function $Q(x)$ has a slope m and intercept b given by

$$m = 2/\sigma^2$$

$$b = -2x_0/\sigma^2. \qquad (5-12)$$

Solving for σ^2 and x_0 gives

$$\sigma^2 = 2/m$$

$$x_0 = -b/m . \qquad (5-13)$$

Equation 5-14 gives the expressions for the slope m and the intercept b of the line fit to the set of points [x, Q(x)] by the weighted-least-squares method: (*5-14*)

The estimated variance of $Q(x)$ is a function only of the uncertainties in $y(x)$:

$$\sigma^2[Q(x)] = \sigma_r^2[y(x-1)] - \sigma_r^2[y(x-1)] \qquad (5-15)$$

where $\sigma_r(y) \equiv \sigma(y)/y$.

If the background continuum is small enough to ignore, then the variance becomes

$$\sigma^2[y(x)] \approx 1/y(x) . \qquad (5-16)$$

if the background continuum is subtracted by the straight-line procedure later shown in Section 5.3.3, the expression for $\sigma^2[y(x)]$ is given by (*5-17*)

Also, $y_i(x)$ is the total counts in channel x and the meanings of the other parameters are given in Section 5.3.3.

For a linear fit there are simple expressions for the estimated variance σ^2 of m and b:

$$\sigma^2(m) \simeq \frac{1}{\Delta}\sum\frac{1}{\sigma_i^2}$$

$$\sigma^2(b) \simeq \frac{1}{\Delta}\sum\frac{x_i}{\sigma_i^2} . \qquad (5-18)$$

Although the fitting procedure just described may seem somewhat complex, the fit can be performed by a short computer program in only a few seconds. The Gaussian function should be fit to the top three-fourths to two-thirds of the peak to avoid problems with non-Gaussian tails and imprecise data. The n channels in the peak give $n - 2$ values of $Q(x)$. When at least four or five values of $Q(x)$ are used in the fit, the results are more than adequate to determine the peak centroids needed for the energy calibration. Unfortunately, it is very difficult to estimate the statistical uncertainty in x_0 using this fitting procedure. However, experience indicates that for peaks of reasonable precision, the values of x_0 are good to ~0.1 channel or better.

In automated operations, a test should be made to determine whether a Gaussian function adequately describes the input data. The reduced chi-square statistic χ^2/ν provides such a test. For the linear fit of $Q(x)$ versus x, (*5-19*)

where m and b are computed from Equation 5-14 and n is the number of values of $Q(x)$ in the fit. For good fits, χ^2/ν should be ~1.00. (See Ref. 5 for a very readable discussion of the properties of χ^2/ν.) For low-precision peaks (up to ~10 000 counts/channel), χ^2/ν is really ~1.00 for peaks of

1

The points of reference of the objects (equations) being inserted are flagged with "(* eq. no. *)" — for example, (*5-14*).

On the first page of the "before" example, the equations flow correctly up until Eq. 5-14. This equation did not appear after its reference because of its size; thus, it was moved to the top of the next page. Equation 5-17 is referenced in the right column and placed two lines below its reference. This could have been corrected by use of the `\refinsertadj` dimension register. Equation 5-19 was too large to fit after its reference and thus was moved to the top of the next page.

The only two-column-spanning equations that were set correctly in the "before" example are Eqs. 5-22 and 5-24, which occur on page 3.

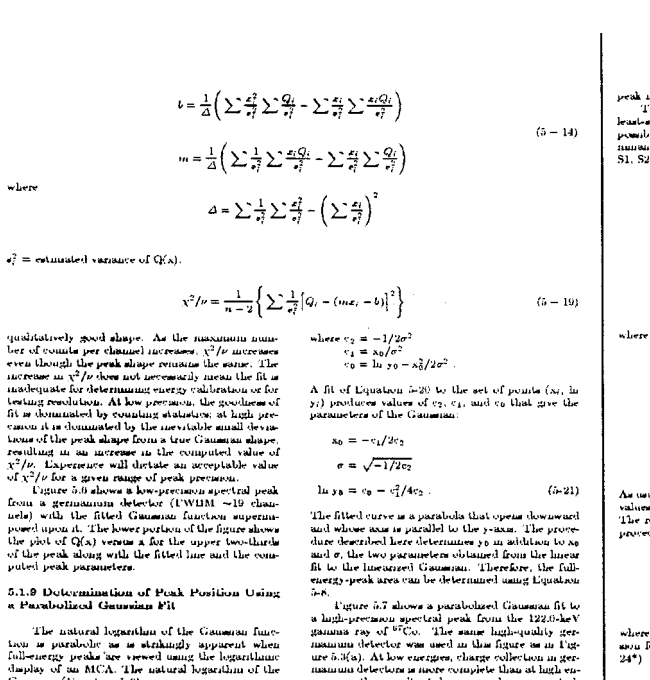

$$b = \frac{1}{\Delta}\left(\sum\frac{x_i^2}{\sigma_i^2}\sum\frac{Q_i}{\sigma_i^2} - \sum\frac{x_i}{\sigma_i^2}\sum\frac{x_iQ_i}{\sigma_i^2}\right)$$

$$m = \frac{1}{\Delta}\left(\sum\frac{1}{\sigma_i^2}\sum\frac{x_iQ_i}{\sigma_i^2} - \sum\frac{x_i}{\sigma_i^2}\sum\frac{Q_i}{\sigma_i^2}\right) \qquad (5-14)$$

where

$$\Delta = \sum\frac{1}{\sigma_i^2}\sum\frac{x_i^2}{\sigma_i^2} - \left(\sum\frac{x_i}{\sigma_i^2}\right)^2$$

σ_i^2 = estimated variance of $Q(x)$.

$$\chi^2/\nu = \frac{1}{n-2}\left\{\sum\frac{1}{\sigma_i^2}\left[Q_i - (mx_i - b)\right]^2\right\} \qquad (5-19)$$

qualitatively good shape. As the maximum number of counts per channel increases, χ^2/ν increases even though the peak shape remains the same. The increase in χ^2/ν does not necessarily mean the fit is inadequate for determining energy calibration or for testing resolution. At low precision, the goodness of fit is dominated by counting statistics; at high precision it is dominated by the inevitable small deviations of the peak shape from a true Gaussian shape, resulting in an increase in the computed value of χ^2/ν. Experience will dictate an acceptable value of χ^2/ν for a given range of peak precision.

Figure 5.6 shows a low-precision spectral peak from a germanium detector (FWHM ~19 channels) with the fitted Gaussian function superimposed upon it. The lower portion of the figure shows the plot of $Q(x)$ versus x for the upper two-thirds of the peak along with the fitted line and the computed peak parameters.

5.1.9 Determination of Peak Position Using a Parabolized Gaussian Fit

The natural logarithm of the Gaussian function is parabolic as is strikingly apparent when full-energy peaks are viewed using the logarithmic display of an MCA. The natural logarithm of the Gaussian (Equation 5-6) gives

$$ln\,y = c_2\,x^2 - c_1\,x - c_0 \qquad (5-20)$$

where $c_2 = -1/2\sigma^2$
$c_1 = x_0/\sigma^2$
$c_0 = \ln y_0 - x_0^2/2\sigma^2$.

A fit of Equation 5-20 to the set of points $(x_i, \ln y_i)$ produces values of c_2, c_1, and c_0 that give the parameters of the Gaussian:

$$x_0 = -c_1/2c_2$$

$$\sigma = \sqrt{-1/2c_2}$$

$$\ln y_0 = c_0 - c_1^2/4c_2 . \qquad (5-21)$$

The fitted curve is a parabola that opens downward and whose axis is parallel to the y-axis. The procedure described here determines y_0 in addition to x_0 and σ, the two parameters obtained from the linear fit to the linearized Gaussian. Therefore, the full-energy-peak area can be determined using Equation 5-8.

Figure 5.7 shows a parabolized Gaussian fit to a high-precision spectral peak from the 122.0-keV gamma ray of ^{57}Co. The same high-quality germanium detector was used in this figure as in Figure 5.3(a). At low energies, charge collection in germanium detectors is more complete than at high energies, with a resultant decrease in low-energy tailing. Comparison of Figures 5.3(a) and 5.7 shows that the tailing in the 122-keV peak of Figure 5.7 is even less than the small tailing of the 1332-keV

2

peak in Figure 5.3(a).

The expressions for the weighted quadratic least-squares fit are included for the convenience of possible users. The expressions are given in determinant form and involve eight sums, indicated by S1, S2, ..., S8. (*5-22*)

$$c_0 = \frac{1}{\Delta}\begin{vmatrix} S6 & S2 & S3 \\ S7 & S3 & S4 \\ S8 & S4 & S5 \end{vmatrix}$$

$$c_1 = \frac{1}{\Delta}\begin{vmatrix} S1 & S6 & S3 \\ S2 & S7 & S4 \\ S3 & S8 & S5 \end{vmatrix} \qquad (5-22)$$

$$c_2 = \frac{1}{\Delta}\begin{vmatrix} S1 & S2 & S6 \\ S2 & S3 & S7 \\ S3 & S4 & S8 \end{vmatrix}$$

where

$$\Delta\begin{vmatrix} S1 & S2 & S3 \\ S2 & S3 & S4 \\ S3 & S4 & S5 \end{vmatrix}$$

$$S1 = \sum\frac{1}{\sigma_i^2} \quad S2 = \sum\frac{x_i}{\sigma_i^2} \quad S3 = \sum\frac{x_i^2}{\sigma_i^2} \quad S4 = \sum\frac{x_i^3}{\sigma_i^2}$$

$$S5 = \sum\frac{x_i^4}{\sigma_i^2} \quad S6 = \sum\frac{ln\,y_i}{\sigma_i^2} \quad S7 = \sum\frac{x_i\,ln\,y_i}{\sigma_i^2} \quad S8 = \sum\frac{x_i^2\,ln\,y_i}{\sigma_i^2} .$$

As usual, the sums are over all the points fit. The y_i values have the background continuum subtracted. The remaining expressions required for the fitting procedure are

$$\sigma_i = \sigma(ln\,y_i)$$

$$\sigma(ln\,y) = \frac{\sigma(y)}{y\,ln\,y} \qquad (5-23)$$

where $\sigma(y)$ is given by Equation 5-17. The expression for χ^2/ν, the goodness-of-fit statistic, is (*5-24*)

$$\chi^2/\nu = \frac{1}{n-3}\left\{\frac{1}{\sigma_i^2}\left[ln\,y_i - (c_2x_i^2 - c_1x_i - c_0)\right]\right\} \qquad (5-24)$$

where n is the number of points fit and c_2, c_1, and c_0 are the values computed from Equation 5-22.

The remarks made in the previous section about the portion of the peak to be fit and about trends in χ^2/ν values apply equally well here. The quadratic fits put considerable demands on the computer, and occasionally the six significant decimal digits provided by many 16-bit processors running in single precision are insufficient for performing correct quadratic fits on high-precision data.

5.1.10 Determination of Peak Position Using Complex Spectral Fitting Codes

Large fitting codes are used to analyze complex spectra with overlapping peaks. The codes describe the peaks with functions that have a basic Gaussian form, with tailing functions added to describe the peak shape more accurately. An iterative nonlinear least-squares procedure is used to fit the data. The centroid of the Gaussian component of the fitted peak is taken as the peak position for purposes of energy determination.

3

```
                                        %      material in TeX's memory
\beginmulcolinsert{r}{2}{1}{pg.no.}  % r=right here, 2=spans two columns,
 1=starts
                                        % in 1st column, pg.no.=on this page #
the object                              % Equation, figure, table, text, or
 combination
\endmulcolinsert                        % End of the object and single column mode
```

In addition to the objects discussed above, the fizzrev macro package formats a journal's title page, figure captions (including figures inserted with the psfig macro package), three levels of section headings, and textual references and numbers for equations (using a placeholder instead of an equation number). The line lengths of the title and running heads are both user-adjustable. See the listing below for definitions of available macros in the fizzrev package.

Using the two-column macros from inside one's own macros makes writing macros like `\refrule` easier; neither the macro designer nor the user needs to worry about the details of getting out of two-column mode to center the rule. The following coding was required to implement the reference rule:

```
\def\refrule{                          % Begin def
   \phyrevfalse                        % Don't draw reading flow indicators here
   \beginmulcolinsert{r}{2}{1}{0}      % r=the rule is an insert, 2=spanning
                                       %          two columns, 1=starting in the
                                       %          left column, 0=on current page
   \vskip2pc                           % Leave some white space
   \centerline{\vrule width16.5pc depth0pt height.5pt}     % Center the line
   \vskip1.5pc                         % Leave more white space
   \endmulcolinsert                    % End of insert
   \phyrevtrue                         % Set indicators back on
}
```

4.5 Fizzrev Macro Definitions

Following each definition, is an example of how to use the macro in a paper. See the Fizzrev Users Guide for complete descriptions.[1]

`\abstract{}`: formats the abstract. The argument is the text of the abstract.
`\abstract{This is an abstract.}`

`\affil{}`: for the name of the author's affiliation. The argument is the name of the affiliation.
`\affil{Los Alamos National Laboratory}`

`\authors{}`: used when there is more than one author/affiliation pair.
`\authors{Jane Doe}\affil{Sandia National Laboratory}`

`\autoauthorfalse` or `true`: switch for user control of running author headline. It is set true in the fizzrev package to enable automatic generation of a running author headline on even-numbered pages. `\authauthorfalse` will cause the macros to prompt the user for a running author headline.

`\autotitlefalse` or `true`: switch for user control of running title headline. It is set true in the fizzrev package to enable automatic generation of a running title headline on odd-numbered pages. `\autotitlefalse` will cause the macros to prompt the user for a running title headline.

[1] Available from the authors.

\beginmc{}{}: abbreviation for the multi-column **\beginmulcol** macro. **\beginmc{2}{20.5pc}**

\binsert{}{}{}{}: abbreviation for the multi-column **\beginmulcolinsert** macro. **\binsert{r}{2}{1}{2}** "Place it right here, span 2 columns, start in 1st column, and put the object on page 2."

\bttp: abbreviation for the multi-column **\balancetothispoint** macro.

\einsert: abbreviation for the multi-column **\endmulcolinsert** macro.

\endmc: abbreviation for the multi-column **\endmulcol** macro.

\eq: used to reference an equation in the text and number it. **``See Equation \eq{\qa}. A + B = C \eqno(\qa).''** **\qa** is just a placeholder, the **\eq** macro will evaluate the placeholder to the current number stored in the equation counter.

\fig{}{}{}{}: used to set the caption and leave space for the figure. Argument 1 is the height of the figure, argument 2 is the width of the figure, argument 3 is the caption excluding a label (i.e., Fig. 1), and argument 4 is a switch for a box outline (set to 1 for on, 0 for off). **\fig{20pc}{20.5pc}{This is a caption.}{1}**

\figcount: used to control the figure number. **\figcount=3** to get a figure labelled "Fig. 4".

\getheaderfooterinfo{}{}{}{}: provides the information for the header and the footer. Argument 1 is the volume number, argument 2 is the issue number, argument 3 is the title, and argument 4 is the author's name. **\getheaderfooterinfo{12}{35}{Title}{Author}**

\it: used for standard italics text. **\it{emphasis}**

\jtp: used to set a journal titlepage and page parameters. See also **\ptp**.

\letter{}: used for figures that are lettered, i.e., Fig. 1A. The argument is the needed letter. **\letter{A}**

\ninepoint: for text and math at nine point. Shouldn't be needed but it is available. **{\ninepoint This text will be in 9-point.}**

\page{}: used instead of **\pageno** macro. The argument is the first page of the journal or the paper. **\page{1}**

\phyrevfalse or **true**: switch that controls the drawing of reading flow indicators, true for on, false for off. Set to true in the fizzrev package.

\postscriptfig{}{}{}: for use with PSFIG macro package. Argument 1 is the height of the figure, argument 2 is the width of the figure, argument 3 is the figure caption, excluding a label (i.e., Fig. 1), and argument 4 is the name of the PostScript file. **\postscriptfig{20pc}{20.5pc}{This is a caption.}{figure1.ps}**

\ptp: for a paper's title page. Will set up the **\vsize** and the headline size for a paper.

\recvd{}: argument is a date. The word "Received" and the opening and closing parentheses are added by the macros and centered. **\recvd{3 March 1989}**

`\refrule`:	centers a rule before the references, leaving white space before and after the rule.
`\rm`:	for times roman font. Ten point default font for text.
`\rauthorhsize`:	the hsize for the running author headline. Defaults to 32 picas. `\rauthorhsize=28pc`
`\rtitlehsize`:	the `\hsize` for the running title headline. Defaults to 27 picas. `\rtitlehsize=28pc`
`\section{}`:	for a level one -heading. Argument is the heading, will be centered in bold and set in all caps automatically. Macro will leave the appropriate vertical spacing. `\section{This is a section heading}`
`\subsection{}`:	for a level-two heading. Argument is the heading, will be centered in bold. Macro will leave the appropriate vertical spacing. User must type the argument using mixed case. `\subsection{This is a subsection heading}`
`\subsubsection{}`:	for a level-three heading. Argument is the heading and it will be centered in italics. Macro will leave the appropriate vertical spacing. User must type the argument using mixed case. `\subsubsection{This is a subsubsection heading}`
`\tenpoint`:	the default point size used for a paper. Shouldn't be needed but it is available.
`\titlehsize`:	the `\hsize` used for the title on the titlepage of the paper. Defaults to 38 picas. `\titlehsize=36pc`

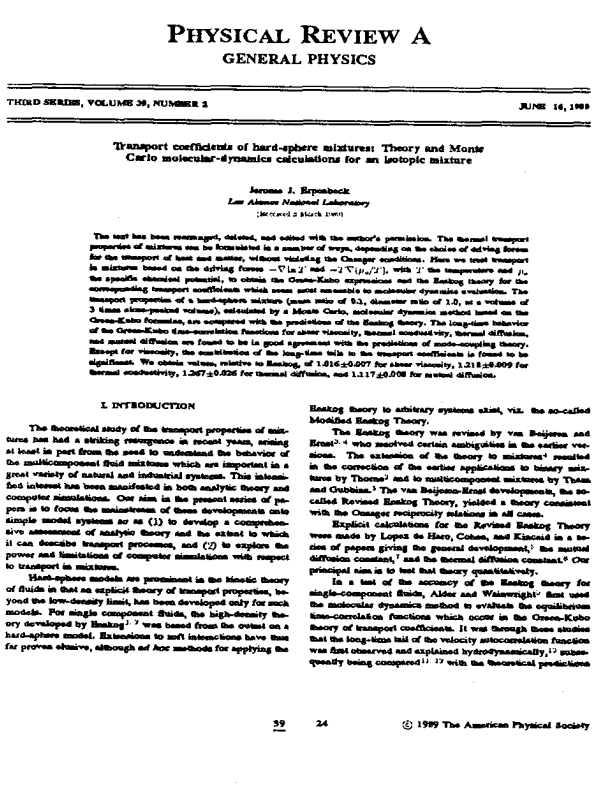

PHYSICAL REVIEW A
GENERAL PHYSICS

THIRD SERIES, VOLUME 39, NUMBER 2 JUNE 16, 1989

Transport coefficients of hard-sphere mixtures: Theory and Monte Carlo molecular-dynamics calculations for an isotopic mixture

Jerome J. Erpenbeck
Los Alamos National Laboratory

The text has been rearranged, deleted, and edited with the author's permission. The thermal transport properties of mixtures can be formulated in a number of ways, depending on the choice of driving forces for the transport of heat and matter, without violating the Onsager conditions. Here we treat transport in mixtures based on the driving forces $-\nabla \ln T$ and $-T\nabla(\mu_a/T)$, with T the temperature and μ_a the specific chemical potential, to obtain the Green-Kubo expressions and the Enskog theory for the corresponding transport coefficients which some recent measures to molecular dynamics evaluation. The transport properties of a hard-sphere mixture (mass ratio of 9:1, diameter ratio of 1:0, at a volume of 3 times close-packed volume), calculated by a Monte Carlo, molecular dynamics method based on the Green-Kubo formulas, are compared with the predictions of the Enskog theory. The long-time behavior of the Green-Kubo time-correlation functions for shear viscosity, thermal conductivity, thermal diffusion, and mutual diffusion are found to be in good agreement with the predictions of mode-coupling theory. Except for viscosity, the contribution of the long-time tails to the transport coefficients is found to be significant. We obtain values, relative to Enskog, of 1.016±0.007 for shear viscosity, 1.218±0.009 for thermal conductivity, 1.267±0.026 for thermal diffusion, and 1.117±0.008 for mutual diffusion.

I. INTRODUCTION

The theoretical study of the transport properties of mixtures has had a striking resurgence in recent years, arising at least in part from the need to understand the behavior of the multicomponent fluid mixtures which are important in a great variety of natural and industrial systems. This intensified interest has been manifested in both analytic theory and computer simulations. Our aim in the present series of papers is to focus the mainstream of these developments onto simple model systems so as (1) to develop a comprehensive assessment of analytic theory and the extent to which it can describe transport processes, and (2) to explore the power and limitations of computer simulations with respect to transport in mixtures.

Hard-sphere models are prominent in the kinetic theory of fluids in that an explicit theory of transport properties, beyond the low-density limit, has been developed only for such models. For single component fluids, the high-density theory developed by Enskog[1,2] was based from the outset on a hard-sphere model. Extensions to soft interactions have thus far proven elusive, although *ad hoc* methods for applying the Enskog theory to arbitrary systems exist, viz. the so-called Modified Enskog Theory.

The Enskog theory was revised by van Beijeren and Ernst[3,4] who resolved certain ambiguities in the earlier versions. The extension of the theory to mixtures[5] resulted in the correction of the earlier applications to binary mixtures by Thorne[6] and to multicomponent mixtures by Thorne and Gubbins.[7] The van Beijeren-Ernst developments, the so-called Revised Enskog Theory, yielded a theory consistent with the Onsager reciprocity relations in all cases.

Explicit calculations for the Revised Enskog Theory were made by Lopez de Haro, Cohen, and Kincaid in a series of papers giving the general development,[8] the mutual diffusion constant,[9] and the thermal diffusion constant.[9] Our principal aim is to test that theory quantitatively.

In a test of the accuracy of the Enskog theory for single-component fluids, Alder and Wainwright[10] first used the molecular dynamics method to evaluate the equilibrium time-correlation functions which occur in the Green-Kubo theory of transport coefficients. It was through these studies that the long-time tail of the velocity autocorrelation function was first observed and explained hydrodynamically,[11,12] subsequently being compared[11,12] with the theoretical predictions

39 24 © 1989 The American Physical Society

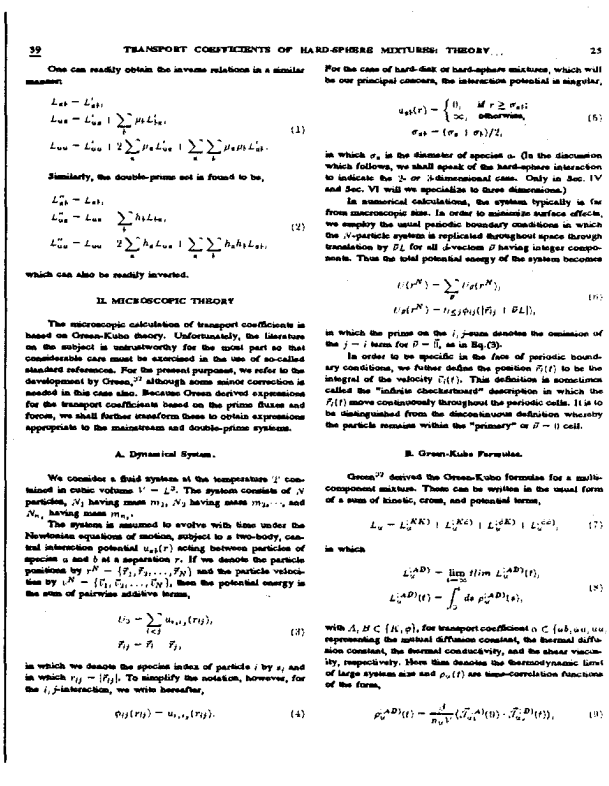

39 TRANSPORT COEFFICIENTS OF HARD-SPHERE MIXTURES: THEORY... 25

One can readily obtain the inverse relations in a similar manner:

$$L_{ab} = L'_{ab},$$
$$L_{ua} = L'_{ua} + \sum_b \mu_b L'_{ba},$$
$$L_{uu} = L'_{uu} + 2\sum_a \mu_a L'_{ua} + \sum_a \sum_b \mu_a \mu_b L'_{ab}. \quad (1)$$

Similarly, the double-prime set is found to be,

$$L''_{ab} = L_{ab},$$
$$L''_{ua} = L_{ua} + \sum_b h_b L_{ba},$$
$$L''_{uu} = L_{uu} + 2\sum_a h_a L_{ua} + \sum_a \sum_b h_a h_b L_{ab}, \quad (2)$$

which can also be readily inverted.

II. MICROSCOPIC THEORY

The microscopic calculation of transport coefficients is based on Green-Kubo theory. Unfortunately, the literature on the subject is untrustworthy for the most part so that considerable care must be exercised in the use of so-called standard references. For the present purposes, we refer to the development by Green,[22] although some minor correction is needed in this case also. Because Green derived expressions for the transport coefficients based on the prime fluxes and forces, we shall further transform these to obtain expressions appropriate to the mainstream and double-prime systems.

A. Dynamical System.

We consider a fluid system at the temperature T contained in cubic volume $V = L^3$. The system consists of N particles, N_1 having mass m_1, N_2 having mass m_2, ..., and N_α, having mass m_α.

The system is assumed to evolve with time under the Newtonian equations of motion, subject to a two-body, central interaction potential $u_{ab}(r)$ acting between particles of species a and b at a separation r. If we denote the particle positions by $r^N = \{\vec{r}_1, \vec{r}_2, \ldots, \vec{r}_N\}$ and the particle velocities by $v^N = \{\vec{v}_1, \vec{v}_2, \ldots, \vec{v}_N\}$, then the potential energy is the sum of pairwise additive terms,

$$U_\Phi = \sum_{i<j} u_{s_i s_j}(r_{ij}),$$
$$\vec{r}_{ij} = \vec{r}_i - \vec{r}_j, \quad (3)$$

in which we denote the species index of particle i by s_i and in which $r_{ij} = |\vec{r}_{ij}|$. To simplify the notation, however, for the i,j-interaction, we write hereafter,

$$\phi_{ij}(r_{ij}) = u_{s_i s_j}(r_{ij}). \quad (4)$$

For the case of hard-disk or hard-sphere mixtures, which will be our principal concern, the interaction potential is singular,

$$u_{ab}(r) = \begin{cases} 0, & \text{if } r \geq \sigma_{ab}; \\ \infty, & \text{otherwise}, \end{cases}$$
$$\sigma_{ab} = (\sigma_a + \sigma_b)/2, \quad (5)$$

in which σ_a is the diameter of species a. (In the discussion which follows, we shall speak of the hard-sphere interaction to indicate the 2- or 3-dimensional case. Only in Sec. IV and Sec. VI will we specialize to three dimensions.)

In numerical calculations, the system typically is far from macroscopic size. In order to minimize surface effects, we employ the usual periodic boundary conditions in which the N-particle system is replicated throughout space through translation by $\vec{p}L$ for all d-vectors $\vec{p}$ having integer components. Thus the total potential energy of the system becomes

$$U(r^N) = \sum_{\vec{p}} U_{\vec{p}}(r^N),$$
$$U_{\vec{p}}(r^N) = U_{\vec{0}} \sum_{i,j} \phi_{ij}(|\vec{r}_{ij} + \vec{p}L|), \quad (6)$$

in which the prime on the i,j-sum denotes the omission of the $j = i$ term for $\vec{p} = \vec{0}$, as in Eq.(3).

In order to be specific in the face of periodic boundary conditions, we further define the position $\vec{r}_i(t)$ to be the integral of the velocity $\vec{v}_i(t)$. This definition is sometimes called the "infinite checkerboard" description in which the $\vec{r}_i(t)$ move continuously throughout the periodic cells. It is to be distinguished from the discontinuous definition whereby the particle remains within the "primary" or $\vec{p} = 0$ cell.

B. Green-Kubo Formulas.

Green[22] derived the Green-Kubo formulas for a multicomponent mixture. These can be written in the usual form of a sum of kinetic, cross, and potential terms,

$$L_{ij} = L_{ij}^{(KK)} + L_{ij}^{(KC)} + L_{ij}^{(CC)}, \quad (7)$$

in which

$$L_{ij}^{(AD)} = \lim_{t\to\infty} t \lim_{L\to\infty} L_{ij}^{(AD)}(t),$$
$$L_{ij}^{(AD)}(t) = \int_0^t ds\, \rho_{ij}^{(AD)}(s), \quad (8)$$

with $A, B \in \{K, C\}$, for transport coefficient $i \in \{ab, au, uu, \eta\}$ representing the mutual diffusion constant, the thermal diffusion constant, the thermal conductivity, and the shear viscosity, respectively. Here time denotes the thermodynamic limit of large system size and $\rho_{ij}(t)$ are time-correlation functions of the form,

$$\rho_{ij}^{(AD)}(t) = \frac{1}{n_a V}\langle \vec{J}_{ai}^{(A)}(0) \cdot \vec{J}_{aj}^{(B)}(t)\rangle, \quad (9)$$

mode-coupling theory, as developed by Ernst *et al.*,[15,16,17] and considered the mainstream and double-prime systems in addition to the prime hydrodynamics of Pomeau. Because the form of the mode-coupling results depends on the form of the starting hydrodynamic equations, it is evident that the long-time tails for a given set of time-correlation functions will have different forms when expressed in terms of the different set of transport coefficients.

Wood[22] considered the case of a binary mixture in 3-dimensions, assuming that the equation of state and transport coefficients are known. In addition to confirming, except for numerous apparent misprints, the results of Pomeau[20] for the long-time tails in the prime system of forces and forces, he also obtained relatively simple expressions for the tails for the double-prime system and somewhat more complicated expressions for the mainstream system. In this section we display the mode-coupling results for the latter.

The general form of the long-time tail for transport coefficient L_α is

$$p_\alpha(t) \sim k_\alpha t^{-d/2}. \tag{10}$$

It is perhaps simplest to write the coefficient k_α in terms of the double-prime transport coefficients rather than the mainstream coefficients. For mutual diffusion, then, the coefficient is

$$k_{11} = \frac{d}{d\pi^{d/2}\mu_\sigma(\eta_+ \quad \eta_-)} \sum_{\pm=+,-} \frac{\eta_\pm \quad L''_{00}/c_p/T'}{[4\pi(\eta \mp \eta_\pm)/\rho]^{d/2}} \tag{11}$$

in which

$$\eta_\pm = \frac{1}{2}(\mu_\sigma L''_{11} + L''_{00}/c_p/T' \pm \mathcal{D}^{\frac{1}{2}}),$$
$$\mathcal{D} = \left(\frac{L''_{00}}{c_p/T} - \mu_\sigma L''_{11}\right)^2 + 4\frac{\mu_\sigma}{c_p/T}(L''_{01})^2, \tag{12}$$
$$\mu_\sigma = \left(\frac{\partial(\mu_1 \quad \mu_2)}{\partial c_1}\right)_{T,p}$$

and in which c_p is the specific constant-pressure heat capacity. For thermal diffusion, the coefficient is

$$k_{01} = \frac{d}{d\mu_\sigma\pi^{d/2}(\eta_+ \quad \eta_-)} \frac{c_p/T'}{L''_{01}} \sum_{\pm=+,-} \frac{(\eta_\pm \quad L''_{00}/c_p/T')(\eta_\pm \quad \mu_\sigma L''_{11} + (h_1 \quad h_2)L''_{01}/c_p/T')}{[4\pi(\eta \mp \eta_\pm)/\rho]^{d/2}} \tag{13}$$

For thermal conductivity, the long-time tail coefficient is

$$k_{00} = \frac{c^2}{d\pi^{d/2}(4\pi\Gamma_1)^{d/2}} + \frac{d}{d\mu_\sigma\pi^{d/2}(\eta_+ \quad \eta_-)} \left(\frac{c_p/T}{L''_{01}}\right)^2 \sum_{\pm=+,-} \frac{(\eta_\pm \quad L''_{00}/c_p/T')(\eta_\pm \quad \mu_\sigma L''_{11} + (h_1 \quad h_2)L''_{01}/c_p/T')^2}{[4\pi(\eta \mp \eta_\pm)/\rho]^{d/2}}, \tag{14}$$

in which c is the adiabatic sound speed,

$$c^2 = \left(\frac{\partial p}{\partial \rho}\right)_{s,c_1}, \tag{15}$$

and Γ_1 is the acoustic damping constant,

$$\Gamma_1 = \frac{1}{\rho}\left[\frac{2(d \quad 1)}{d}\eta + \zeta\right] + \Gamma_{00}$$
$$\Gamma_{00} = \frac{\gamma \quad 1}{\rho c_p T'}\left[L''_{00} \quad 2\frac{\rho c_p T'\mu_\sigma}{\chi}L''_{01} + \left(\frac{\rho c_p T'\mu_\sigma}{\chi}\right)^2 L''_{11}\right], \tag{16}$$

in which

$$\chi = \frac{T'}{\rho}\left(\frac{\partial \rho}{\partial T'}\right)_{p,c_1} \tag{17}$$

is related to the usual volume coefficient of thermal expansion and

$$\mu_\sigma = \left(\frac{\partial(\mu_1 \quad \mu_2)}{\partial p}\right)_{T,c_1}. \tag{18}$$

By virtue of Eq.(2) relating the double-prime transport coefficients to the mainstream coefficients, we regard these expressions as providing the mainstream long-time tails in terms of the mainstream transport coefficients.

III. MONTE CARLO, MOLECULAR DYNAMICS CALCULATIONS

In this section, we discuss the evaluation of the transport coefficients directly from the Green-Kubo formulas for a 50:50 binary mixture of hard spheres ($d = 3$), each species having diameter σ, but the particles of species having a mass of $0.1m_1$. Because the thermodynamic and transport variables have a trivial dependence on temperature for hard spheres, we specify the state through the volume relative to

We have used the highest "Enskog approximation" (i.e., highest degree Sonine polynomial expansion) for which the

FORTRAN package was designed, namely the tenth approximation.

In similar fashion, we determine the long-time tails of the time-correlation functions from these double-prime transport coefficients, obtaining the required thermodynamic quantities. For example, to obtain μ_σ we use

$$\left(\frac{\partial \mu_\sigma}{\partial c_1}\right)_{T,p} = \sum_i \left(\frac{\partial \mu_\sigma}{\partial n_i}\right)_{T,\{n_{i\neq 1}\}} \left(\frac{\partial n_i}{\partial c_1}\right)_{T,p},$$
$$\left(\frac{\partial n_1}{\partial c_1}\right)_{T,p} = \frac{1}{J_2}\left(\frac{\partial p}{\partial n_2}\right)_{T,n_1},$$
$$\left(\frac{\partial n_2}{\partial c_1}\right)_{T,p} = \frac{1}{J_2}\left(\frac{\partial p}{\partial n_1}\right)_{T,n_2},$$
$$J_2 = \frac{m_1 m_2}{(m_1 n_1 + m_2 n_2)^2}\sum_s n_s \left(\frac{\partial p}{\partial n_s}\right)_{T,\{n_{i\neq s}\}},$$
$$\bar{p}_s = \mu_s \quad \frac{\pi}{6}p\sigma_s^3/m_s, \tag{19}$$

which can be readily evaluated.

A. Numerical Results

Our calculations include the study of systems of 108, 500, 1372, and 4000 particles. The parameters for each of these calculations are given in Table I, including the time-steps per trajectory $N_{t\mu}$ and the number of trajectories N_{tr}. Observe that for the larger systems the trajectories are relatively short on the basis of the number of collisions per particle. Because the number of trajectories for the larger systems is not proportionately larger, the calculations for the larger systems, especially the 4000-particle system, are relatively less extensive when applied to the calculation of time-correlation functions for the transport properties studied here.

Our results consist of the time-dependent transport coefficients, either evaluated directly from, as in the case of mutual diffusion and thermal diffusion, or through differentiation, of the Einstein function, as in the case of the thermal conductivity and the viscosity. We define reduced transport coefficients relative to the Enskog values (in the tenth Sonine approximation) by adding a carat over the symbol, e.g.,

$$\hat{L}_\alpha = L_\alpha/L^E_\alpha. \tag{20}$$

The Enskog transport coefficients are evaluated as outlined above, yielding

$$L^E_{00} = 3.9197430\frac{m_1}{(m_1\beta)^{1/2}\sigma_1^2},$$
$$L^E_{01} = \quad 0.054992\frac{m_1}{(m_1\beta)^{1/2}\sigma_1^2},$$
$$L^E_{11} = 0.0021164\frac{m_1(m_1\beta)^{1/2}}{\sigma_1^2}, \tag{21}$$
$$L^E_\eta = 0.2937862\frac{m_1}{(m_1\beta)^{1/2}\sigma_1^2},$$

In similar fashion we define a reduced time relative to the mean free time,

$$\hat{t} = t/t_0, \tag{22}$$

which we estimate numerically from the collision rate,

$$t_0 = \left\langle \frac{t_i N(N \quad 1)}{2N_c} \right\rangle, \tag{23}$$

in which N_c is the number of collisions on a trajectory extending to time t_i. The observed values of t_0 relative to the Boltzmann expression, are given in Table I.

The time-dependent thermal conductivity for the 500-particle system is shown as a function of time in Fig. 1. The arrow in the figure marks the time $t_a = L/c$ required for an acoustic wave to transverse the 500-particle system. For self-diffusion, finite-system effects were found to become important for larger values of the time.[12] The form of the dependence on time is similar to that shown by the other transport coefficients, except at early times. (The fact that, for hard spheres, the time-dependent transport coefficients for certain transport properties are non-zero at $t = 0$ is related to the presence of δ-functions in the corresponding microscopic current; we will discuss this further in a future article.) The values of $L_\alpha(t_f)$, the transport coefficients at the longest times considered in these calculations, are given in Table I. For each transport coefficient, these values are plotted against $1/N$ in Fig. 2 to show the approach to the thermodynamic limit. The least-squares fit of the results to a $1/N$ form yields values for the thermodynamic limit given in Table II. The least-squares lines are also shown in Fig. 2.

Agreement remains adequate. Note that the theoretical tail is quite small in this case and that the time-correlation function appears to be indistinguishable from zero over most of the range of time which is displayed.

To estimate the complete transport coefficient, we add the mode-coupling long-time tail contribution, starting at a time t_{m1} to the infinite-system extrapolation for $L_\alpha(t_{m1})$, where t_{m1} is sufficiently large so that the difference between the mode-coupling prediction and the large-system limit of the actual tail is negligible. Our comparisons in Fig. 3 6 suggest that t_{m1} should be at least $35t_0$. In Table II, we show the results for two choices for t_{m1} viz., about $35t_0$ and the longest time t_f for which $L_\alpha(t)$ is computed, as previously discussed. In each case, we assign a statistical uncertainty to the final estimate, based on the uncertainty in $L_\alpha(t_{m1})$. Because this uncertainty increases with time, it is evident that the choice, $t_{m1} = 35t_0$, will lead to a smaller uncertainty. Nonetheless the results from these two choices are in statistical agreement. In view of the agreement suggested by Fig. 3 6, the $t_{m1} = 35t_0$ estimate would appear to be justified although the magnitude of the systematic error cannot be estimated by the sample approach.

FIG. 1. Time-dependent thermal conductivity, relative to the Enskog value, for a 50:50 binary hard-sphere mixture having mass ratio of 0.1 and diameter ratio of 1.0 at a volume of three times close packing, as a function of the time t, relative to the observed mean free time t_0, for a 500-particle system. The arrow shows the acoustic wave traversal time for the system. The error bars represent ± 1 standard deviation about the mean.

IV. CONCLUSIONS

We list here what seem to be the most important conclusions that can be drawn from this work.

1. The transport coefficients for mixtures can be defined in a variety of ways by virtue of the fact that the separation of the heat current into a thermal and a diffusive part is not unique, even when subject to the Onsager conditions. From the point of view of molecular dynamics calculations, the mainstream choice of fluxes and forces, with driving forces of $\nabla^{-1}\nabla T$ and $T\nabla(\mu_\sigma/T)$, yields Green-Kubo expressions which do not require knowledge of the partial specific enthalpies for the system and so, therefore, more easily applied.

2. For the mass and diameter ratio studied here at a volume of 3 times close-packing, the long-time behavior of the time-correlation functions for shear viscosity, thermal conductivity, thermal diffusion, and mutual diffusion appear to agree (within their statistical uncertainties) with the predictions of the mode-coupling theory. Except for the strong evidence for agreement in the case of one-component self-diffusion,[11,12] the present evidence seems to be the first to support mode-coupling theory for other time-correlation functions. Whether this agreement holds for other densities and for other mass and diameter ratios remains to be seen.

3. The results for the hard-sphere transport coefficients for the isotopic mixture show significant deviations from the Enskog theory. These deviations arise principally from the

FIG. 2. Reduced transport coefficients for a 50:50 binary hard-sphere mixture having mass ratio of 0.1 and diameter ratio of 1.0, evaluated at a time t_f (see Table I) of approximately 100 mean free times, as a function of the reciprocal of the total number of particles N, showing the dependence on system size. The various transport coefficients are $\alpha = \mu\mu$ for thermal conductivity, $\mu\mu$ for mutual diffusion, 11 for mutual diffusion, and η for shear viscosity. The lines are a weighted linear least-squares fit for each set of data. To avoid confusion, the error bars (± 1 standard deviation) are not shown for all of the $N = 4000$ data; see Table I for the values.

long-time tails of the time correlation functions, as can be seen from Table II. The values of $L_\alpha(35t_0)$ show quite modest deviations from unity, even though the time is long compared to the Enskog decay time. The additional contributions for longer times are small for shear viscosity, but increasingly large for mutual diffusion (7%), thermal diffusion (11%), and thermal conductivity (15%). This result contrasts with the conclusion of Alder and Wainwright[18] for the thermal conductivity of a single-component, hard-sphere fluid but agrees with their observations for shear viscosity.

4. The present results suggest that further study of the parameter space for hard-sphere mixtures is in order. Calculations for other densities and for a number of other mass and diameter ratios are now in progress.

ACKNOWLEDGMENT

The author is grateful to W. W. Wood of Carroll College for extensive discussion of the mixture problem and for making his results for the long-time tails available before publication. He is also grateful to J. M. Kincaid of the State University of New York at Stony Brook, E. G. D. Cohen

of Rockefeller University, and M. Lopez de Haro of Instituto de Investigaciones en Materiales, Universidad Nacional Autonoma de Mexico for numerous discussions and for providing the evaluation of the Enskog transport coefficients and their help in modifying these programs to yield the desired form of the coefficients.

This work was supported by a contract with the U. S. Department of Energy, Office of Basic Energy Sciences, Division of Chemical Sciences.

1. D. K. Enskog, Svenska Vetenskapsakad. Handl. 63, 4 (1922).
2. S. Chapman and T. G. Cowling, *The Mathematical Theory of Nonuniform Gases*, Cambridge University Press, Cambridge, 1952. Second edition.
3. H. van Beijeren and M. H. Ernst, Physica 68, 437 (1973).
4. H. van Beijeren and M. H. Ernst, Physica 70, 225 (1973).
5. M. K. Theis and K. E. Gubbins, J. Chem. Phys. 55, 268 (1971).
6. M. Lopez de Haro, E. G. D. Cohen, and J. M. Kincaid, J. Chem. Phys. 78, 2746 (1983).
7. J. M. Kincaid, M. Lopez de Haro, and E. G. D. Cohen, J. Chem. Phys. 79, 4509 (1983).
8. J. M. Kincaid, E. G. D. Cohen, and M. Lopez de Haro, J. Chem. Phys. 86, 967 (1987).
9. B. J. Alder and T. E. Wainwright, Phys. Rev. Lett. 18, 988 (1967).
10. B. J. Alder and T. E. Wainwright, Phys. Rev. A 1, 18 (1970).
11. J. J. Erpenbeck and W. W. Wood, Phys. Rev. A 26, 1648 (1982).
12. J. J. Erpenbeck and W. W. Wood, Phys. Rev. A 32, 412 (1985).
13. J. R. Dorfman and E. G. D. Cohen, Phys. Rev. A 6, 776 (1972).
14. J. R. Dorfman and E. G. D. Cohen, Phys. Rev. A 12, 292 (1975).
15. M. H. Ernst, E. H. Hauge, and J. M. J. van Leeuwen, Phys. Rev. A 4, 2055 (1971).
16. M. H. Ernst, E. H. Hauge, and J. M. J. van Leeuwen, J. Stat. Phys. 15, 7 (1976).
17. M. H. Ernst, E. H. Hauge, and J. M. J. van Leeuwen, J. Stat. Phys. 15, 23 (1976).
18. B. J. Alder, D. M. Gass, and T. E. Wainwright, J. Chem. Phys. 53, 3813 (1970).
19. T. R. Kirkpatrick, Phys. Rev. Lett. 53, 1735 (1984).
20. I. M. de Schepper, A. F. Haffmans, and H. van Beijeren, Phys. Rev. Lett. 57, 1715 (1986).
21. G. Jacucci and I. R. McDonald, Physica A 80, 607 (1975).
22. C. Hoheisel and U. Deiser, Mol. Phys. 37, 95 (1979).
23. A. A. Clifford and B. Dickinson, Mol. Phys. 34, 875 (1977).
24. D. L. Jolly and R. J. Bearman, Mol. Phys. 41, 137 (1980).
25. M. Schoen and C. Hoheisel, Mol. Phys. 52, 33 (1984).
26. M. Schoen and C. Hoheisel, Mol. Phys. 52, 1029 (1984).
27. R. Vogelsang and C. Hoheisel, Phys. Rev. A 35, 3487 (1987).
28. D. MacGowan and D. J. Evans, Phys. Rev. A 34, 2133 (1986).
29. S. R. de Groot, *Thermodynamics of Irreversible Processes*, North-Holland, Amsterdam, 1951.
30. W. W. Wood, Mode-Coupling Theory for the Long-Time Tails for the Transport Coefficients of Mixtures, (in preparation).
31. S. R. de Groot and P. Mazur, *Nonequilibrium Thermodynamics*, North-Holland, Amsterdam, 1962.
32. H. S. Green, J. Math. Phys. 2, 344 (1961).
33. Y. Pomeau, J. Chem Phys. 57, 2800 (1972).
34. J. J. Erpenbeck and W. W. Wood, J. Stat. Phys. 24, 455 (1981).
35. J. M. Kincaid, (private communication).
36. J. M. Kincaid and J. J. Erpenbeck, *The Mutual Diffusion Constant of Binary Isotopic Hard-Sphere Mixtures: Molecular Dynamics Calculations using the Green-Kubo and Steady State Methods*, 1986.

5. What Next?

1. We need to simplify the TEX code for these macros and make it smaller. It would be nice if PCs and Macintoshes could use it.
2. We want to start processing flowing text as objects.
3. There is a need for one- and two-column footnotes.
4. Document the code.
5. Port the "place it here" code to three columns so it could be used for other formats.

6. A Comment on the Future of TEX

TEX must be enhanced with multiple-column formatting, object-placement options, and other related commands if it is to remain viable in the years ahead. WYSIWYG systems (such as Interleaf and Frame) that combine WYSIWYG with batch formatting in an effort to allow users to use tags for Standard Generalized Markup Language (SGML), will be tough competition for TEX as it now stands. In addition to these features, math formatting will soon be offered by Frame.

With content tagging (SGML) soon to be a way of life for most of us as we enter the age of knowledge information processing, a good batch formatting system in the public domain would be of great value. We would like that system to be TEX. We have a lot of TEX experience to draw upon. However, the program can't perform the tasks its competitors are beginning to be able to address.

Some of the other enhancments we would like to see include:

1. An input file that could be buffered so that processing could be done on the contents of the buffer. A command such as `\inputbuffersize`*2000* would establish the size of the buffer in bytes.
2. The ability to do string searches on the contents of the buffer and process the buffer up to the point a string match was found. It would also be useful if string searches could be done on the contents of any box and the match point returned. Commands such as `\vsplit\mybox to` `\findstring`{*string arg*}would then be possible.
3. The ability to write the contents of the unprocessed buffer to another file.
4. The ability to write contents of any box or delineated string to an ASCII file.
5. The ability to create multiple `dvi` output files.
6. The ability to assign a variable as a real, as well as a dimension or count register. Full floating-point arithmetic would be available on these variables.